UNIVERSITATEA "POLITEHNICA" din BUCUREȘTI
FACULTATEA DE ȘTIINȚE APLICATE
Nr. Decizie _____ din _____

TEZĂ DE DOCTORAT

Collective properties of rare-earth nuclei: Lifetime measurements using recoil distance Doppler shift technique

(Proprietăţi colective ale nucleelor pământurilor rare: măsurări de timp de viaţă utilizând tehnica deplasării Doppler)

Doctorand: Ing. Fiz. **Turturică Andrei Emanuel**

COMISIA DE DOCTORAT

Președinte	Prof. Dr. Cristina STAN	de la	Univ. Politehnica București
Conducător de doctorat	Prof. Dr. Gheorghe CĂTA-DANIL	de la	Univ. Politehnica București
Referent	Prof. Dr. Mircea-Iacob GIURGIU	de la	Univ. Tehnică de Construcţii București
Referent	CS I Dr. Nicolae Marius MĂRGINEAN	de la	INCD Fizică și Inginerie Nucleară ,,Horia Hulubei"
Referent	CS II Dr. Constantin MIHAI	de la	INCD Fizică și Inginerie Nucleară ,,Horia Hulubei"

BUCUREȘTI 2021

Contents

1 Introduction **4**

2 Theoretical models **5**
2.1 Shell model 6
2.2 Collectivity 7
2.3 The five-dimensional collective Hamiltonian - 5DCH model 8

3 Lifetime measurements at the 9MV Tandem Accelerator **9**
3.1 Introduction 9
3.2 The 9MV Tandem Accelerator 9
3.3 The ROSPHERE Array of Detectors 10
3.4 Recoil Distance Doppler Shift Method 11

4 Struture investigation in ^{136}Nd **14**
4.1 Introduction 14
4.2 Experimental Setup 14
4.3 Results 16
4.4 Results interpretation 17

5 Struture investigation in ^{154}Er **18**
5.1 Introduction 18
5.2 Experimental setup 18
5.3 Results 20
5.4 Angular correlations measurements 21
5.5 Results interpretation 22

List of Figures

1 The Shell model level scheme showing the level succession and formation of the shells corresponding the magic numbers 2, 8, 20, 28, 50, 82, 126, and 184. Figure taken from [1] 6

2 The famous Casten triangle highlighting the main limits of the geometric model and the $R_{4/2}$ ratio, respectively. Figure taken from [2] 7

3 Picture of the ROSPHERE spectrometer in the 25 HPGe configuration. 11

4 The recoil distance Doppler shift schematic showing the basics of the method. Figure taken from [3] 12

5 The Koln design of the recoil distance Doppler shift plunger reaction chamber. Figure taken from [4] 13

6 Partial level scheme of ^{136}Nd that highlights the levels of interest for this analysis. The intensities of the transitions are the ones observed in the experiment. The lifetimes shown represent all lifetimes measured using Doppler shift techniques 15

7 Mean lifetime for the 2_1^+, 4_1^+, 7_1^-, 9_1^- states for each distance measured in the forward direction (37°) and 14_1^+ state measured in the backward direction (143°). The horizontal lines are the weighted average of these values and its uncertainty. Normalised values of the S-component (black circles) and U-component (red squares) of the $2_1^+ \rightarrow 0^+$, $4_1^+ \rightarrow 2_1^+$, $7_1^- \rightarrow 6_1^+$, $9_1^- \rightarrow 7_1^-$ transition intensities measured in the forward direction and $14_1^+ \rightarrow 12_1^+$ transition intensity measured in the backward direction. . . 16

8 The reduced transition probability systematics of the neutron deficient Nd isotopes compared with the predictions provided by the 5DCH model. Figure taken from [5]. 17

9 Partial level scheme of ^{154}Er that highlights the levels of interest for this analysis build based on transitions observed in the experiment. 19

10 Mean lifetime for the 2_1^+, 4_1^+, 6_1^+, 8_1^+, and 10_1^+ states for each distance measured in the forward direction (37°) . The horizontal lines are the weighted average of these values and its uncertainty. Normalised values of the S-component (black circles) and U-component (red squares) of the $2_1^+ \rightarrow 0^+$, $4_1^+ \rightarrow 2_1^+$, $6_1^+ \rightarrow 4_1^+$, $8_1^+ \rightarrow 6_1^+$, and $10_1^+ \rightarrow 8_1^+$ transition intensities measured in the forward direction. 20

11 Partial level scheme of ^{154}Er showing the newly found levels and transitions that could be part of the γ-band 21

12 Angular correlations measurement results obtained for ^{154}Er. The bottom panel shows the fit for the $4_1^+ \rightarrow 2_1^+ \rightarrow 0_1^+$ known cascade that highlights the possible errors in the analysis. The top panel shows the fit for the $2_2^+ \rightarrow 2_1^+ \rightarrow 0_1^+$ newly found cascade. 22

13 The reduced transition probabilities B(E2) calculated using the IBA-1 framework compared with the experimental values measured in this work. 23

List of Tables

1 The ROSPHERE spectrometer detector position angles and the distance from the center of the sphere [6]. 10
2 Lifetimes measured in the present work and the reduced transition probabilities obtained in this analysis. 17
3 Lifetimes measured in the present work. The reduced transition probabilities obtained in this analysis alongside the previously known values. 21

1 Introduction

Rare earth elements are a series of 15 metallic chemical elements with atomic numbers ranging from 57 to 71, also called lanthanides, plus two more elements, scandium, and yttrium with atomic numbers 21 and 39, respectively. These elements have unique chemical properties and are used in many areas of technology and science.

From the nuclear point of view, the rare earth nuclei also exhibit interesting phenomena like the the presence of k-isomers, occurrence of super-deformed structures, or shape coexistence. Also, the nuclear properties exhibited by some rare-earth nuclei are used in several nuclear technology branches. For example, gadolinium is used as an MRI contrast agent, promethium is used in nuclear batteries, ytterbium is used in nuclear medicine and so on. All of these properties require specific research performed in nuclear laboratories to bring new information for testing models developed by our theoretical physics colleagues or to find new properties that can be used in nuclear technologies.

This thesis focuses on the study of collective behavior of two neutron deficient rare earth elements, ^{136}Nd and ^{154}Er, by measuring the lifetimes of low-lying excited nuclear states. The measurements were performed using nuclear spectroscopy techniques and state-of-the-art detector arrays, mechanical devices and electronics, available at the National Institute for Nuclear Physics and Engineering - Horia Hulubei in Bucharest-Magurele (IFIN-HH).

The thesis is structured in six chapters, two consisting of original content on the ^{136}Nd and ^{154}Er isotopes, two consisting of complementary information for the original chapters, introduction, and conclusions.

Chapter 2 is dedicated to briefly explain the basics of the collective models involved in describing the two isotopes studied for this project. Each of the three limits, vibrator, rotor, and γ-soft are outlined. Also, in the end, the five-dimensional collective Hamiltonian model is depicted as it is used to interpret the ^{136}Nd isotope. In chapter 3, I start by describing the present state-of-the-art detector array called ROSPHERE and the detectors used to measure γ rays and charged particles produced in nuclear reactions using stable ion beams delivered by the 9MV TANDEM accelerator. Next, I present the techniques used by the nuclear spectroscopy group in IFIN-HH to measure sub-nanosecond lifetimes, with a comprehensive description of the Recoil distance Doppler shift method (RDDS).

In Chapter 4 the focus is shifted on the original content of this thesis. The lifetimes of nuclear excited states in ^{136}Nd were measured using the RDDS method. This measurement is interesting as it required two more methods alongside the RDDS technique to properly obtain and confirm seven nuclear lifetimes. The experimental results are interpreted using the five-dimensional collective Hamiltonian model. The chapter 5 is dedicated to the measurement of nuclear lifetimes of exited states in ^{154}Er. In this

case, five states were measured and the results were interpreted using the IBA-1 model framework. Moreover, we try to find the second $I^\pi = 2^+$ state that starts the γ-band and the first $I^\pi = 3^-$ state, by using angular correlations measurements. Lastly, in Chapter 6 I summarize the results and present the main conclusions of this thesis.

2 Theoretical models

Until a complete theory explains all phenomena of a physical system, there are usually several iterations that try to describe the physical properties of said system as close as possible. These models typically have to impose some simplifying assumptions that lead to satisfying results. Still, once we stray from those initial presumptions, we obtain results that significantly diverge from experimental observation. This approach is not entirely without purpose as it reveals some pros and cons for the initial assumptions that will lead to a better path in future models. The first theoretical model that explained some experimentally observed properties in nuclei was a collective model, the liquid drop model. The highlight of this model is the semi-empirical formula for obtaining the binding energy of nuclei. As the basis of this model, several facts were used: first, the radius of the nucleus was approximated at $R = r_0 A^{(1/3)}$, the nuclear mass was believed to be incompressible and spherical in shape. Secondly, the average binding energy per nucleon for nuclei with $A < 30$ is rapidly increasing to mass $A = 60$ at 8.8 MeV, with several spikes at nuclei with mass 4, 8, 20, 50, and then slowly decreases. Also, nuclei with a certain number of nucleons: 4, 8, 20, 50, 82, 126, now known as magic numbers, have local spikes in energy. Third, the binding energy is systematically greater for even-even nuclei than odd-odd or even-odd, which suggests the tendency for pairing of identical nucleons. This model's applications were limited, so a new model with a completely new approach became the nuclear physics benchmark. As it was named, the shell model was inspired by the atomic shell model with several minor changes to fit the nuclear landscape. It quickly became the most powerful prediction tool, but it was useful mainly for nuclei near closed shells, where particles are confined to only one J shell. For nuclei between shells, the possible number of configurations can be so significant that it makes calculations practically impossible. The famous nuclear physicist Talmi said that "in the case of ^{154}Sm there are around 3 x 10^{14} states with spin and parity 2^+ that can be constructed with protons and neutrons in the Z = 50 - 82 and N = 82 - 126 shells". Clearly, nuclear physics needed something new, and so the collective model of Bohr and Mottelson was developed.

2.1 Shell model

In atomic shell model the ionisation energy as a function of the number of electrons has a specific pattern with peaks at certain numbers called magic numbers at 2, 10, 18, 36, 54, 86. Analogous in nuclear physics the excitation energy as a function of atomic number Z presents a clear pattern with peaks of extra regional stability at 2, 8, 20, 28, 50, 82 and 126 [7]. This similarity induced the idea of a core comprised of closed shells of protons and neutrons that exert a potential, usually a modified harmonic oscillator potential or a modified square well potential. The nucleons that are outside of the closed shells move freely in this central potential and solely determine the properties of the nucleus.

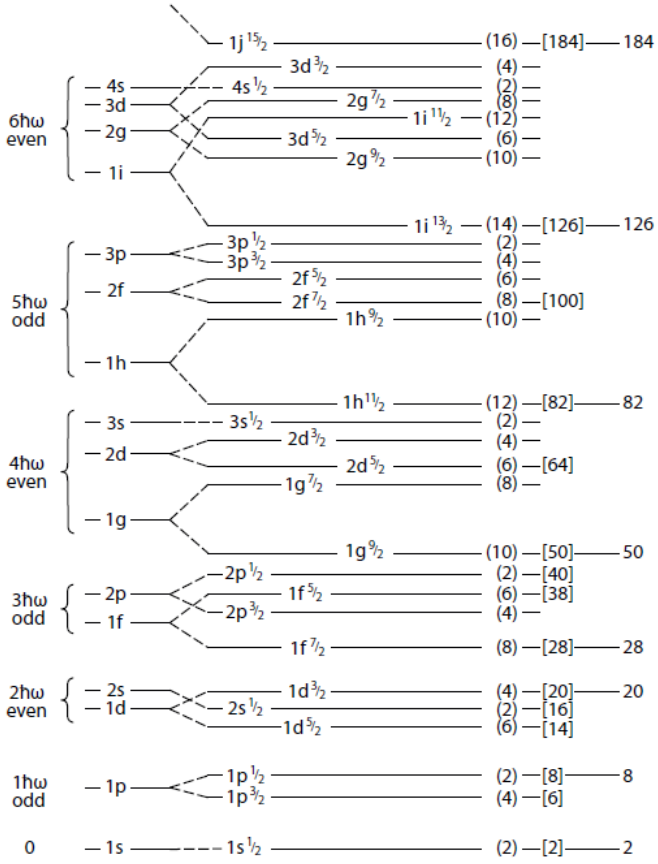

Figure 1: The Shell model level scheme showing the level succession and formation of the shells corresponding the magic numbers 2, 8, 20, 28, 50, 82, 126, and 184. Figure taken from [1].

2.2 Collectivity

The term collectivity comes from the hypothesis that the nucleons move collectively and coherently inside the atomic nucleus. Early in the nuclear structure study, researchers proposed this motion because they believed that the nuclear surface could vibrate in the liquid drop model, slightly changing its spherical shape. One of the fundamental properties of the shell model is that the core consists of inert closed shells. This hypothesis is not entirely correct as there are polarisation forces between the valence nucleons and the ones in the closed shells and pairing forces between nucleons in closed shells. The pairing force gives the nucleus a spherical shape, while the polarisation forces tend to deform the nucleus. The balance between these forces gives the form of the nucleus. This phenomenon is the reason why all nuclei near closed shells are spherical. As we add more nucleons, we have structures that are more prone to deformation. Eventually, we reach a region, usually when the number of nucleons is half of those needed to close the shell, where the nucleus becomes permanently deformed in the ground state.
Usually, there are three limits used in the collective model to describe the nuclear motions. These are idealised limits that we can rarely find in reality, but many nuclei lie within these limits and are perfectly exemplified by the famous Casten triangle in Fig. 2 .

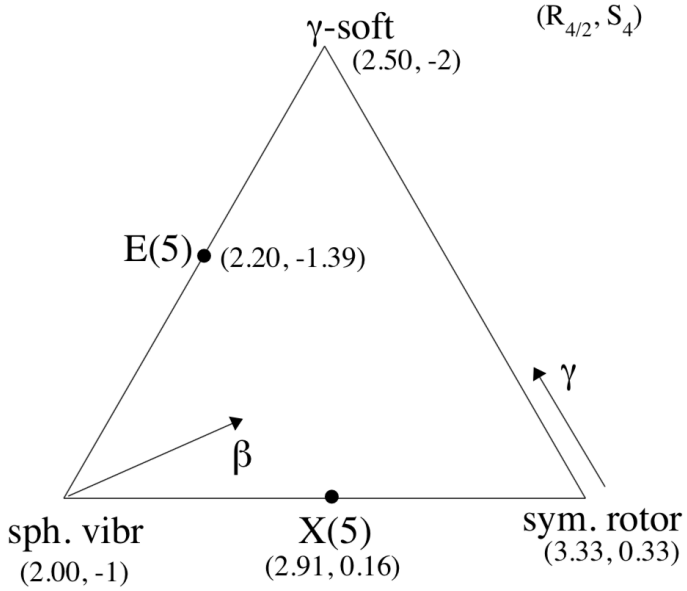

Figure 2: The famous Casten triangle highlighting the main limits of the geometric model and the $R_{4/2}$ ratio, respectively. Figure taken from [2].

2.3 The five-dimensional collective Hamiltonian - 5DCH model

The experimental results obtained in the present study, were interpreted from a theoretical point of view using configuration mixing calculations [8] based on constrained Hartree-Fock-Bogoliubov theory implemented using the D1S Gogny force [9, 10]. The Hartree-Fock method is a computational technique used to determine the the wavefunctions and the energies of a stationary quantum many-body system. This method is widely used to obtain solutions for the Schrodinger equation of atoms, molecules, nano-structures and alongside the Bogoliubov transformation has seen a wide spreed use in nuclear physics. The Pairing energy of nucleons in heavy elements is one of the applications where the Hartree-Fock-Bogoliubov method is used with great success. The Hartree-Fock method states that the many-body wave function of the system can be approximated using a Slater determinant if the system is composed of fermions or by a single permanent of N spin-orbitals if the system is comprised of bosons. The method was developed around 1930 but had limited uses until 1950 due to it's computational demands that could not be satisfied by the technology available at the time. The D1S Gogny force is postulated to be [9]:

$$\begin{aligned} V(r) = & \sum_{i=1,2} (W + BP_\sigma - HP_\tau - MP_\sigma P_\tau)_i e^{-r^2/\mu_i^2} \\ & + t_0(1 + x_o P_\sigma)\rho^\alpha \Big(\frac{r_1 + r_2}{2}\Big)\delta(r_1 - r_2) \\ & + i(W_{LS}(\sigma_1 + \sigma_2)\overleftarrow{\nabla_1 - \nabla_2}\delta(r_1 - r_2)\overrightarrow{\nabla_1 - \nabla_2} \end{aligned} \tag{1}$$

which is the sum of central and spin orbit terms.

The final 5DCH is expressed [8]:

$$\hat{H}_{coll} = \frac{1}{2}\sum_{k=1}^{3}\frac{\hat{J}_k^2}{\jmath_k} - \frac{1}{2}\sum_{m.n=0and2} D^{-1/2}\frac{\partial}{\partial a_m}D^{1/2}(B_{mn})^{-1} \times \frac{\partial}{\partial a_n} + V(a_0, a_2) - \Delta V(a_0, a_2), \tag{2}$$

where $a_0 = \beta cos\gamma$ and $a_2 = \beta \sin\gamma$, and D is the metric. Eigenstates and eigenvalues are obtain by solving the following equation [8]:

$$\hat{H}_{coll}|JM\rangle = E(J)|JM\rangle \tag{3}$$

The orthonormalized eigenstates $|JM\rangle$ with angular momentum J and projections M are expandes as [8]:

$$|JM\rangle = \sum_K g_K^J(a_0, a_2)|JMK\rangle, \tag{4}$$

with $|JMK\rangle$ a superposition of Wigner rotation matrices.

3 Lifetime measurements at the 9MV Tandem Accelerator

3.1 Introduction

The field of nuclear physics is one of the most challenging physics domains in general due to its limitations in observing the motion, interaction, etc., of nucleons inside the nucleus. As a result, the interrelationship between the nuclear strong force and the Coulomb force is not fully understood. Therefore, we lack essential information to describe what is happening inside the nucleus unequivocally. Nuclear spectroscopy is a branch of nuclear physics that tries to obtain sensitive information about nuclear structure by measuring excited nuclei decay. Most notably, the focus is on measuring the lifetime of nuclear states.

Lifetime measurements of excited nuclear states are essential in studying nuclear structure due to the strong connection between nuclear reduced matrix elements, obtained using the measured lifetimes and the nuclear states wave functions. Considering that lifetime values range from attosecond to billion years, researchers developed several methods to measure these values, each preferable for a specific time interval, and some of them extending over quite a few orders of magnitude. The nuclei I am studying are known to have lifetimes in the range of picoseconds and below, so several methods are suitable for this region. The best method is the Recoil Distance Doppler Shift Method (RDDS), which, given the Bucharest laboratory setup in IFIN-HH, is best suited to measure nuclear lifetimes from one picosecond to one nanosecond. Another method used for this lifetime range is the Doppler Shift Attenuation Method, which can measure lifetimes from one femtosecond to one picosecond. Lastly, the Fast Timing Method is suited to measure lifetimes from a few tens of picoseconds to nanoseconds and even microseconds depending on the detection setup.

This chapter will describe the IFIN-HH laboratory methods to measure lifetimes with a special focus on the Recoil Distance Doppler Shift Method used to measure the lifetimes of several excited nuclear states in ^{136}Nd and ^{154}Er. I will also describe the experimental setup employed by the IFIN-HH laboratory to detect the gamma photons emitted by the decaying nucleus.

3.2 The 9MV Tandem Accelerator

The 9 MV FN Pelletron tandem accelerator was built by the High Voltage Engineering Corporation (HVEC) in 1973 and now has a terminal voltage of 9MV. The machine underwent major upgrades starting with 2006. The charging belt was replaced with a more reliable Pelletron system, new ion sources were installed, and all the vacuum and power supply systems were modernized. This accelerator uses a central high-voltage

terminal to accelerate negative ions extracted from ion sources. Once the negative ions reach the center terminal, carbon foils are used to strip the ions of electrons to become positive and then accelerated away from the terminal. The accelerator is equipped with one Cesium sputtering ion source and one duo-plasmatron with Li/Na charge exchange ion source to extract the negative ions. In theory, it can accelerate all types of ions but, so far, the heaviest ion accelerated is ^{63}Cu, and the most used ions are ^{4}He, ^{7}Li, ^{12}C, ^{13}C, ^{16}O and ^{18}O.

3.3 The ROSPHERE Array of Detectors

The experimental data on ^{136}Nd and ^{154}Er featured in this thesis were obtained using the ROSPHERE γ-ray spectroscopy array [6]. In this section, I will describe the entire setup, from detectors to electronics. The array has 25 positions equally distribute on 5 rings as described in Table 1.

Ring no.	θ(degrees)	ϕ(degrees)	Distance Ortec (mm)	Distance Canberra (mm)
1	37	0, 72, 144, 216 and 288	179	210
2	70	36, 108, 180, 252 and 324	186	217
3	90	0, 72, 144, 216 and 288	176	208
4	110	36, 108, 180, 252 and 324	186	217
5	143	0, 72, 144, 216 and 288	179	210

Table 1: The ROSPHERE spectrometer detector position angles and the distance from the center of the sphere [6].

There are four types of detectors currently used in the setup:

- High Purity Germanium detectors equipped with BGO anti-Compton shields, used for detecting γ-rays with great energy resolution (25 detectors)
- La(Br_3)Ce scintillating detectors, used for detecting γ-rays with great timing resolution (10 detectors)
- Liquid scintillating detectors, used for detecting neutrons (5 detectors)
- Solar cells, used for detecting charged particles (Sorcerer setup [11])

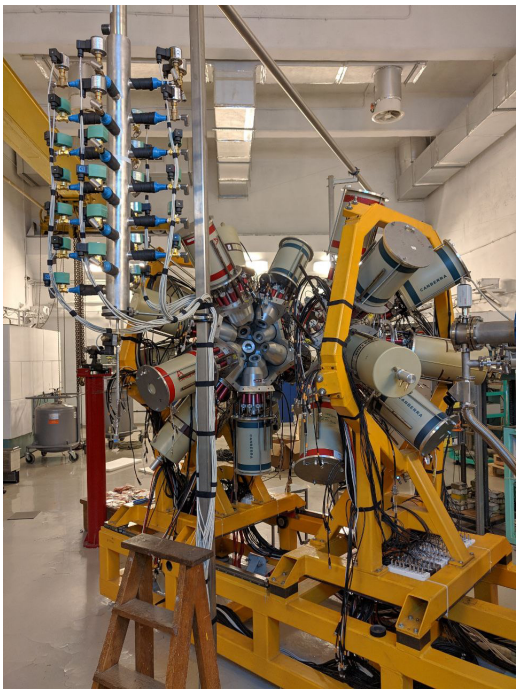

Figure 3: Picture of the ROSPHERE spectrometer in the 25 HPGe configuration.

3.4 Recoil Distance Doppler Shift Method

Nuclear physicists have been using this method for a long time with great success and was constantly improved to match the requirements of the newly developed setup. Today this is the most reliable method for nuclear lifetimes ranging from one picosecond to one nanosecond. It requires highly sophisticated reaction chambers that need to move a target with less than one-micrometer precision using a combination of piezoelectric motors to measure these distances precisely and maintain a high vacuum inside the chamber. These highly demanding mechanical specifications represent one of the significant disadvantages of this method.
Figure 4 is a simplified scheme of the Recoil Distance Doppler Shift Method. The mode of operation is as follows: the nucleus of interest is produced by an accelerated beam of ions incident on a thin target. The newly produced nuclei leave the target with velocities of around 1% of the speed of light. For this reason, the target must be thin enough to permit the nuclei to pass through it and fly towards the stopper, and at the same time, it must be strong enough to maintain its planarity. The stopper has the role of stopping the flying nuclei that we are interested in measuring and letting the beam pass through with minimum interaction.

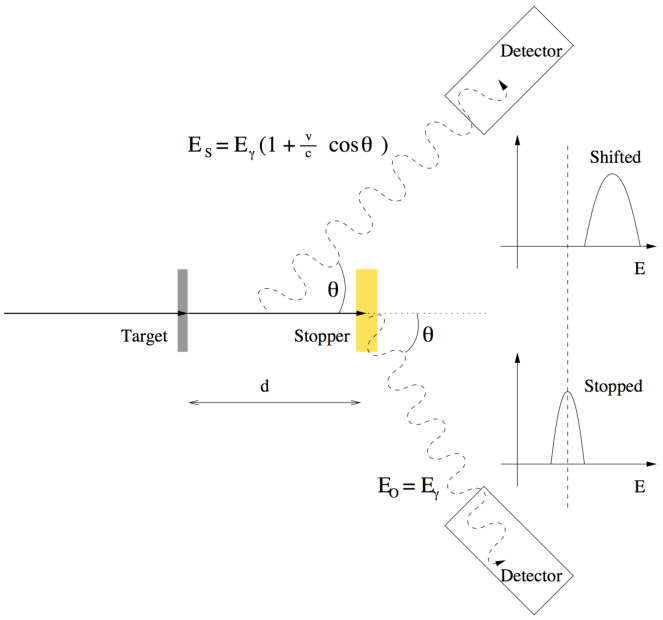

Figure 4: The recoil distance Doppler shift schematic showing the basics of the method. Figure taken from [3].

DDCM for coincidence measurements

Because DDCM applied to coincidence measurements solves several problems, it is only natural that this version is used, with high success, in IFIN-HH laboratory.
In this case, we use a gate to select the decay cascade we are interested in and ensure a unique decay chain. This way, we eliminate all the other direct feeding transitions, so we do not need to worry about the unidentified transitions that might feed our level of interest. At the same time, by gating, we clean the spectra of unwanted gammas. To mathematically describe this, we start from the rate equation for level i, but with only one transition that feeds the level and one that decays it, also known as direct gating [4]:

$$\frac{d}{dt}n_i(t) = -\lambda_i n_i(t) + \lambda_h n_h(t) \tag{5}$$

Solving this equation yields [2]:

$$\tau(x) = \frac{I_{A_U}^{B_S}(x)}{v\frac{d}{dx}I_{A_S}^{B_S}(x)}, \tag{6}$$

where $I_{A_U}^{B_S}$ means the intensity of the unshifted transition A component, gated on the shifted component of transition B. In some cases, like when a transition from the same nucleus with almost the same energy as the transitions we use in direct gating is present, we need to use an indirect gate to remove this contaminant. This means we gate on the transition D from figure 4, and we need to account for the lifetime of the new level, so the lifetime formula becomes [2]:

$$\tau(x) = \frac{I_{A_U}^{C_S}(x) - \alpha I_{B_U}^{C_S}(x)}{v\frac{d}{dx}I_{A_S}^{C_S}(x)}, \tag{7}$$

with:

$$\alpha = \frac{I_{A_U}^{C_S}(x) + I_{A_S}^{C_S}(x)}{I_{B_U}^{C_S}(x) + I_{B_S}^{C_S}(x)}. \tag{8}$$

Plunger device. One of the widely used reaction chambers is the one designed by the Department of Nuclear Physics of Cologne University, and its schematic drawing is represented in Figure 5. This device is called the plunger device due to its shape and is divided into four parts: the target chamber, the bearing unit, the actuator housing, and the adapting piece.

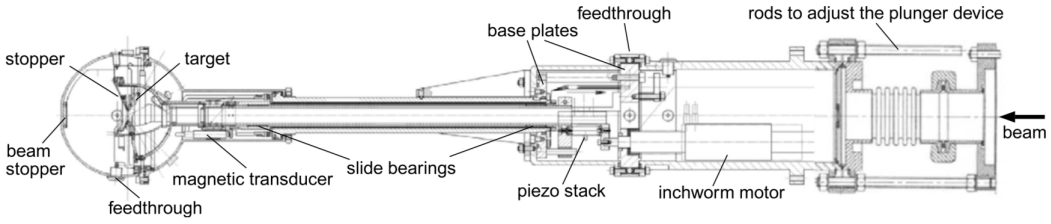

Figure 5: The Koln design of the recoil distance Doppler shift plunger reaction chamber. Figure taken from [4].

The target chamber consists of a rigid support on which the stopper is placed and fixed by screws, a mobile support on which the target is placed and fixed with screws. The bearing unit consists of three concentric tubes, an outer vacuum tube, a middle tube that is fixed on the outer tube with the role of supporting the inner tube held by two bearings at each end. The actuator housing consists of one piezoelectric motor called inchworm, connected to the inner tube that controls the target support's linear motion by performing gross adjustments and another, more sensitive piezo crystal for fine adjustments.

4 Struture investigation in ^{136}Nd

4.1 Introduction

As part of this Ph.D. thesis, which aims to study collectivity in medium mass nuclei, we have proposed an experiment to measure the lifetimes for the low energy Yrast band states in ^{136}Nd. The region containing ^{136}Nd is well known to have a high degree of axial asymmetry and alongside the region centered on ^{108}Ru is the region with the largest deviations from axial symmetry [12]. Researchers have intensively studied these regions, and most of the isotopes have the collective behavior well documented. This was not the case for ^{136}Nd as the lifetime information was scarce. There were known only two lifetimes for the 7^- and 9^- in the negative parity band and several upper limits for the lifetimes of the first 4^+ and 6^+ states [13]. Recently, a coulomb excitation experiment determined the B(E2) of the first 2^+ states in ^{136}Nd [14], but this is almost all experimental information available for this isotope. In this context, the nuclear spectroscopy group of the National Institute of Physics and Nuclear Engineering (IFIN-HH) proposed an experiment at the 9MV Tandem accelerator in Bucharest-Magurele. The experiment objectives were to measure the low lying energy states in the Yrast band of ^{136}Nd up to the 10^+ state and any other possible non-Yrast state with the lifetime in the range of the Recoil Distance Doppler Shift method (RDDS)[4]. Given the Nd neighbors' systematics, we expected the lifetimes that we are interested in to be under 50 ps. Also, using the B(E2) obtained by T.R. Saito et al., we calculated the lifetime for the 2^+ state to be 34(5) ps, which is well within the range for the RDDS method that employs the Doppler effect to measure lifetimes between one ps and one ns. These values will help complete the picture of shape transition in Nd isotopes from deformed (N≈70) to spherical (N≈80) shape. Our group collaborated with J.- P. Delaroche theory group on the ^{138}Nd project, measured one year earlier at the 9 MV tandem accelerator. They provided configuration mixing calculations [8] based on Constrained Hartree-Fock-Bogoliubov (CHFB) calculations implemented using the D1S Gogny force [9, 10] and obtained values for several observables using the five-dimensional collective Hamiltonian (5DCH) that is solved as described in [15]. Given this collaboration's success, they agreed to provide theoretical interpretation on future projects, and ^{136}Nd is a good case as it is interesting for both groups.

4.2 Experimental Setup

The lifetime measurements of ^{136}Nd have been performed at the Horia Hulubei National Institute for Physics and Nuclear Engineering 9 MV Tandem Accelerator in Bucharest - Magurele. The ^{136}Nd nuclei were created in the ^{124}Te(^{16}O,4n) fusion-evaporation reaction using a target produced by the IFIN-HH target laboratory [16], made of ^{124}Te with 0.37 mg/cm^2 thickness deposited on a 3.2 mg/cm^2 gold backing. We used CASCADE

[17] and Compa [18] codes to obtain the cross-section for ^{136}Nd corresponding to the 4n channel. The cross-section is 250 mb obtained at a beam energy of 75 MeV and, for this reason, ^{16}O accelerated at 78 MeV was used to account for the energy loss in the gold backing facing the beam. The recoils had a velocity of 3.02 $\mu m/ps$ ($v/c = 1.01\%$) and the nuclei were stopped using a thick gold foil of 5 mg/cm^2 thickness [5]. $\gamma - \gamma$ coincidence measurements were performed to clean the spectra of unwanted gamma rays resulted from other reaction channels and Coulomb excitation of the gold foils. As a reaction chamber, we used the Koln-Bucharest Plunger Device for its capacity to adjust stopper-target distance with high precision. For detecting the γ-rays, we used the ROSPHERE array of detectors [6] from which we used two rings, each comprising 5 Compton-suppressed 55% HPGe detectors at 37^o and 143^o with respect to the beam direction. We measured at 15 target-stopper distances ranging from 10 to 280 μm [5].

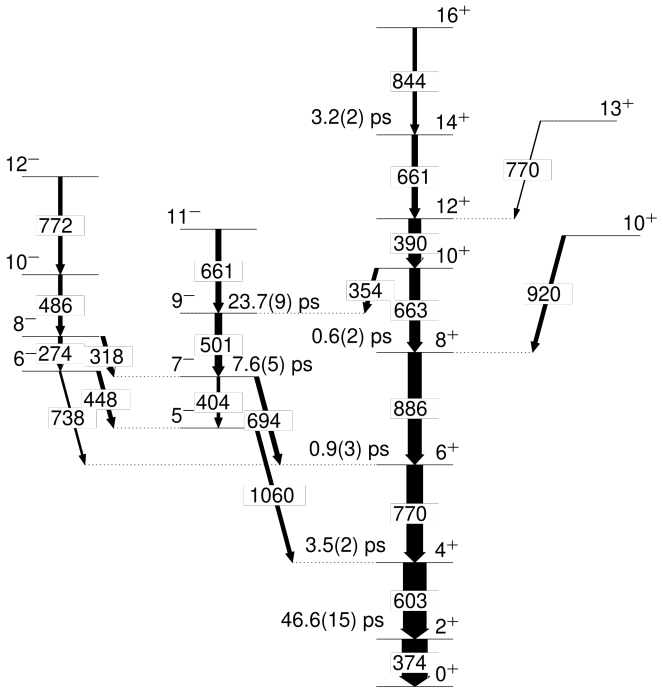

Figure 6: Partial level scheme of ^{136}Nd that highlights the levels of interest for this analysis. The intensities of the transitions are the ones observed in the experiment. The lifetimes shown represent all lifetimes measured using Doppler shift techniques.

4.3 Results

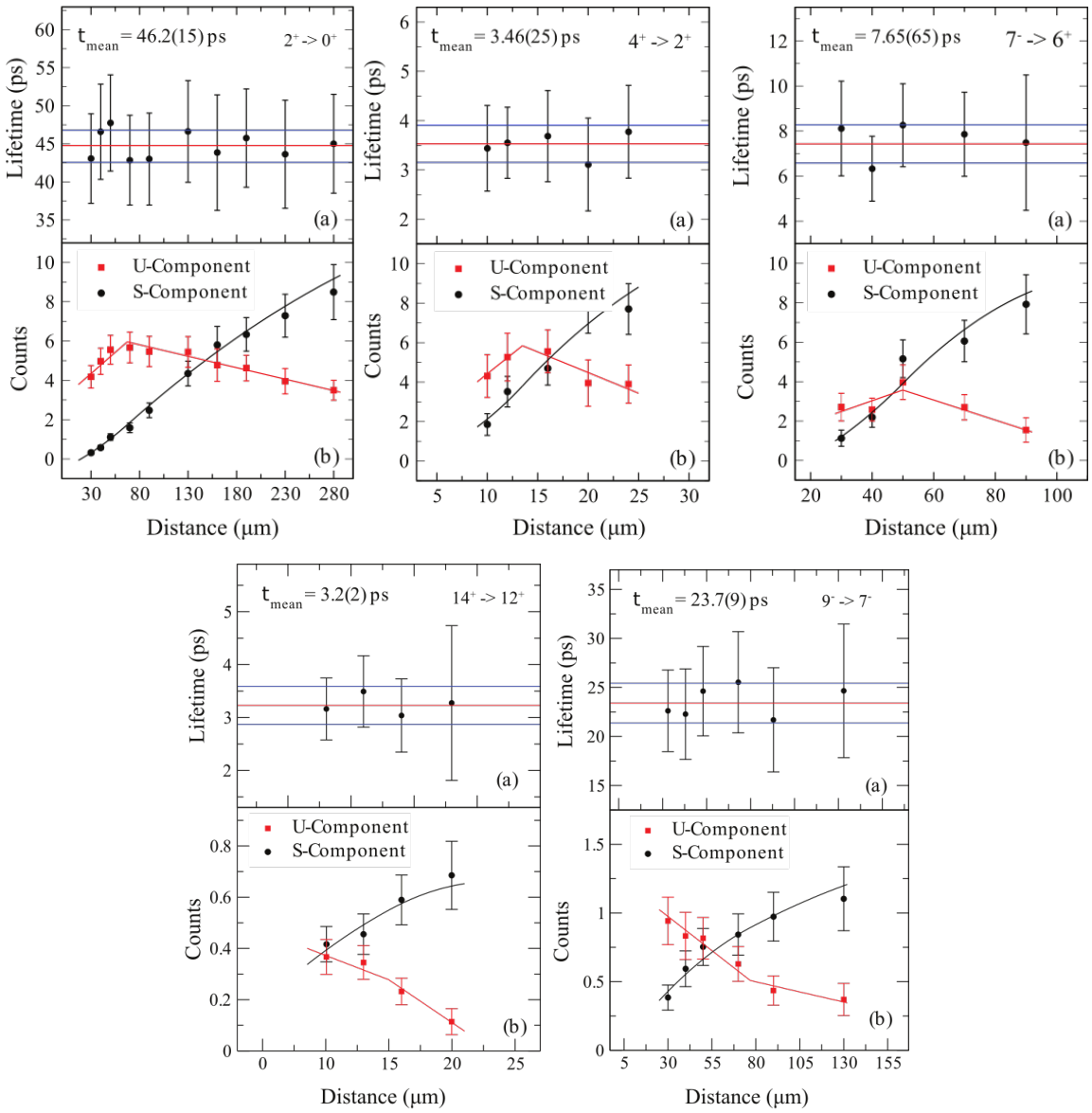

Figure 7: Mean lifetime for the 2_1^+, 4_1^+, 7_1^-, 9_1^- states for each distance measured in the forward direction (37°) and 14_1^+ state measured in the backward direction (143°). The horizontal lines are the weighted average of these values and its uncertainty. Normalised values of the S-component (black circles) and U-component (red squares) of the $2_1^+ \rightarrow 0^+$, $4_1^+ \rightarrow 2_1^+$, $7_1^- \rightarrow 6_1^+$, $9_1^- \rightarrow 7_1^-$ transition intensities measured in the forward direction and $14_1^+ \rightarrow 12_1^+$ transition intensity measured in the backward direction.

$E_x[keV]$	J_n^π	$E_\gamma[keV]$	Gate	$\tau[ps]$	B(E2)[W.u.] (previous)	B(E2)[W.u.] (present)
373.75	2_1^+	373.7	$4_1^+ \rightarrow 2_1^+$	46.2(15)	$80(11)^a$	56.8(19)
976.46	4_1^+	602.7	$6_1^+ \rightarrow 4_1^+$	3.46(25)	$> 21^b$	71(5)
2439.80	7_1^-	404.1	$9_1^- \rightarrow 7_1^-$	7.65(65)	$14(5)^b$	$54(5)^c$
2941.0	9_1^-	501.2	$11_1^- \rightarrow 9_1^-$	23.75(92)	$71(24)^b$	25.9(10)
4347.8	14_1^+	661.3	$16_1^+ \rightarrow 14_1^+$	3.14(27)	$> 27^b$	49(5)

Table 2: Lifetimes measured in the present work and the reduced transition probabilities obtained in this analysis.

4.4 Results interpretation

Our choice of theoretical model is based on the five-dimensional collective Hamiltonian that relies on configuration mixing calculations based on Constrained Hartree-Fock-Bogoliubov calculations implemented using D1S Gogny force [9, 10] described in chapter 2. The model provides predictions for several observables, like the moment of inertia of yrast bands, spectroscopic quadrupole moments, B(E2) strengths, etc. We are interested mostly in the reduced transition probability. The calculated experimental B(E2) strengths are displayed in figure 8 alongside the predicted 5DCH values [5].

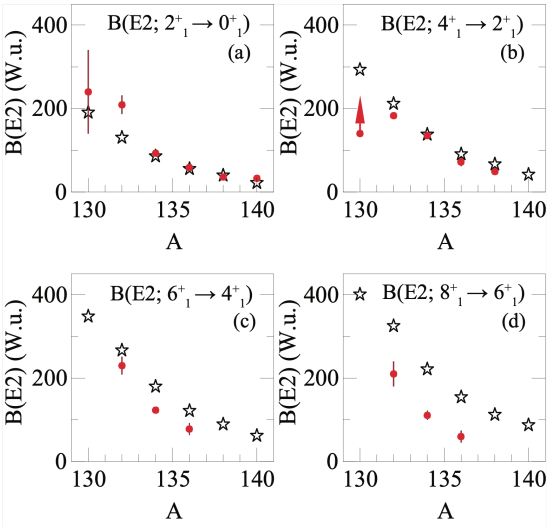

Figure 8: The reduced transition probability systematics of the neutron deficient Nd isotopes compared with the predictions provided by the 5DCH model. Figure taken from [5].

5 Struture investigation in ^{154}Er

5.1 Introduction

The second nucleus studied for my Ph.D. thesis is ^{154}Er. This isotope is a rare-earth nucleus with Z = 68 and N = 86. The rare-earth region has been heavily studied due to its unique particularities in the nuclear structure like the vibrational nature of the low-lying states in the ground state band [19, 20], the occurrence of an island of long lived isomers [21], and the shape transition from prolate to oblate rotation at high spins [22]. Studies have been performed for the Er, Dy, and Gd isotopic chains to understand the nuclear structure under the influence of strong centrifugal and Coriolis fields [23] and found important information about the nuclear shape in the region. Isotones with N $\geq$ 87 were found to exhibit sizable quadrupole deformations, while for N $<$ 87, we are dealing with spherical or weakly oblate nuclei [23]. In the ^{154}Er case, several experiments revealed the superdeformed structure [24, 25] at high spins. Also, the high-spin region has been studied using electron capture experiments [26] and heavy-ion reactions [27, 28, 29] that uncovered the level structure, measured lifetimes of excited nuclear states, and measured the quadrupole moments of coexisting collective shapes at high spin [30]. For the low-lying states, the situation is different as the experimental information is scarce. From the nuclear lifetimes perspective, only the $I^\pi = 11^-$ isomer at 3025 keV has a known lifetime of 39(4) ns. Higher in spin, two experiments measured lifetimes for the negative parity band [28, 29] but had completely different results. Therefore, the values cannot be considered reliable.
Moreover, the level structure is incomplete, with the first $I^\pi = 3^-$ and the second $I^\pi = 2^+$ state not being identified. All of this missing information is valuable from the collective point of view. Given the situation described so far, we decided to measure the lifetimes in the yrast band and try to identify the missing low lying levels. The positive parity levels in the ground state band, up to $I^\pi = 12^+$ are in the range of the RDDS method, while the negative parity states greater than $I^\pi = 13^-$ seem to be in the range of the fast-timing method. Also, angular correlation measurements were performed in order to place any newly discovered level correctly.

5.2 Experimental setup

The lifetime measurements of ^{154}Er have also been performed at the Horia Hulubei National Institute for Physics and Nuclear Engineering 9 MV Tandem Accelerator in Bucharest-Magurele. The ^{154}Er nuclei were produced in the ^{144}Sm(^{13}C,3n) fusion-evaporation nuclear reaction using a target manufactured by the IFIN-HH target laboratory [16]. The target was made of ^{144}Sm with a 0.37 mg/cm^2 thickness deposited on a 3.2 mg/cm^2 gold backing. For cross-section calculations we used CASCADE [17]

and Compa [18] codes. The cross-section is 200 mb obtained at projectile energy of 59 MeV. The beam was accelerated at 60 MeV to account for the energy loss in the gold backing. The recoil velocity was calculated to be 1.91 μm/ps ($v/c = 0.65\%$). The stopper was a thick gold foil of 4.5 mg/cm^2 thickness. Being an RDDS experiment, the Koln-Bucharest Plunger Device was used as a reaction chamber. For γ ray detection, we used the ROSPHERE array of detectors [6] comprising at that time of 14 HPGe germanium detectors placed on four rings at 37^o (five detectors), 90^o (three detectors), 110^o (one detector), and 143^o (five detectors), with the remaining slots filled with $LaBr_3$(Ce) scintillating detectors. We measured at 11 target-stopper distances ranging from 8 μm to 50 μm.

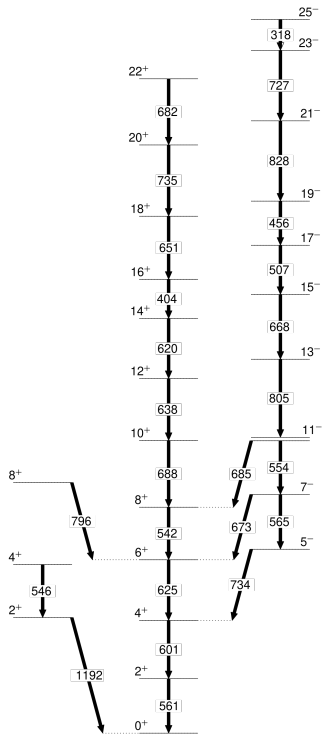

Figure 9: Partial level scheme of ^{154}Er that highlights the levels of interest for this analysis build based on transitions observed in the experiment.

5.3 Results

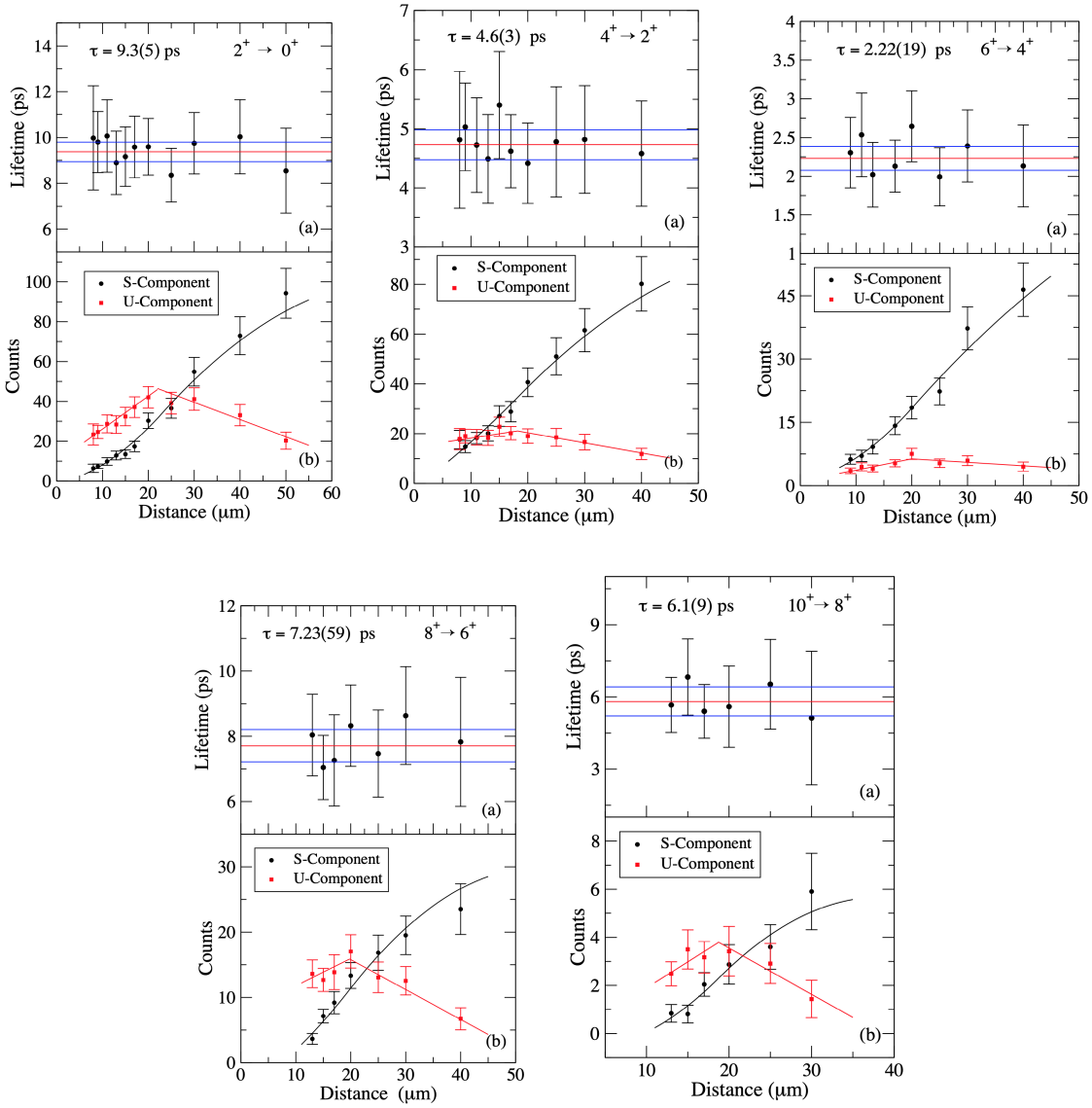

Figure 10: Mean lifetime for the 2_1^+, 4_1^+, 6_1^+, 8_1^+, and 10_1^+ states for each distance measured in the forward direction (37°) . The horizontal lines are the weighted average of these values and its uncertainty. Normalised values of the S-component (black circles) and U-component (red squares) of the $2_1^+ \rightarrow 0^+$, $4_1^+ \rightarrow 2_1^+$, $6_1^+ \rightarrow 4_1^+$, $8_1^+ \rightarrow 6_1^+$, and $10_1^+ \rightarrow 8_1^+$ transition intensities measured in the forward direction.

$E_x[keV]$	J_n^π	$E_\gamma[keV]$	Gate	$\tau[ps]$	B(E2)[W.u.] (present)
560.9	2_1^+	560.9	$4_1^+ \rightarrow 2_1^+$	9.3(5)	31.9(17)
1162.2	4_1^+	601.4	$6_1^+ \rightarrow 4_1^+$	4.6(3)	45.6(30)
1787.6	6_1^+	625.5	$8_1^+ \rightarrow 6_1^+$	2.22(19)	77.7(67)
2329.5	8_1^+	541.9	$10_1^+ \rightarrow 8_1^+$	7.23(59)	48.7(40)
3016	10_1^+	687.8	$12_1^+ \rightarrow 10_1^+$	6.1(9)	17.8(26)

Table 3: Lifetimes measured in the present work. The reduced transition probabilities obtained in this analysis alongside the previously known values.

5.4 Angular correlations measurements

An important aspect in studying the collective behavior of medium mass nuclei is the start of the γ-band, i.e., the second $I^\pi = 2^+$ state. In the case of ^{154}Er, the states in the γ-band were unknown before this experiment, and one of our objectives was to find these missing states. Figure 11 shows the level scheme build by using transitions observed in the current experiment. We used $\gamma - \gamma$ and $\gamma - \gamma - \gamma$ coincidence matrices to identify the decay patterns accurately. The transitions in the left cascade were arranged to be consistent with the previously known level scheme, and we believe this is the right level structure for the γ-band. The next step consists in assigning spin and parities for these newly found levels.

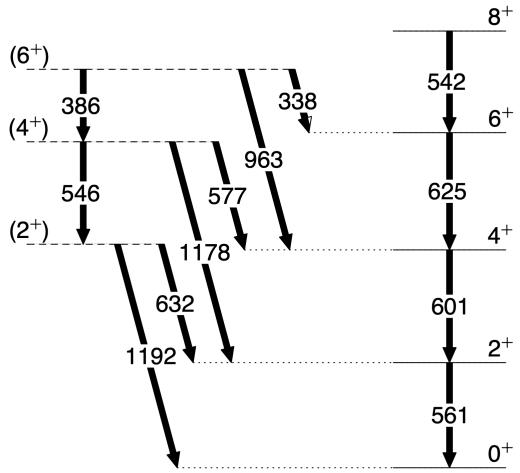

Figure 11: Partial level scheme of ^{154}Er showing the newly found levels and transitions that could be part of the γ-band.

Minor errors in detector angle are present due to mounting problems or angular coverage of the detector. This can be seen in the $4_1^+ \rightarrow 2_1^+ \rightarrow 0_1^+$ measurement, using the 601.4 keV and 560.8 keV transitions, displayed in Figure 12 (bottom panel). This analysis was performed on levels with known spin, parity and mixing ratios to test the experimental setup, and data for any errors that might appear. Two angles at 53 degrees and 144 degrees seem to exhibit significant errors, and, unfortunately, we could not identify the source of these errors. The 144-degree pair is susceptible to errors as there are only two pairs, but the 53-degree has six pairs and should not have problems.

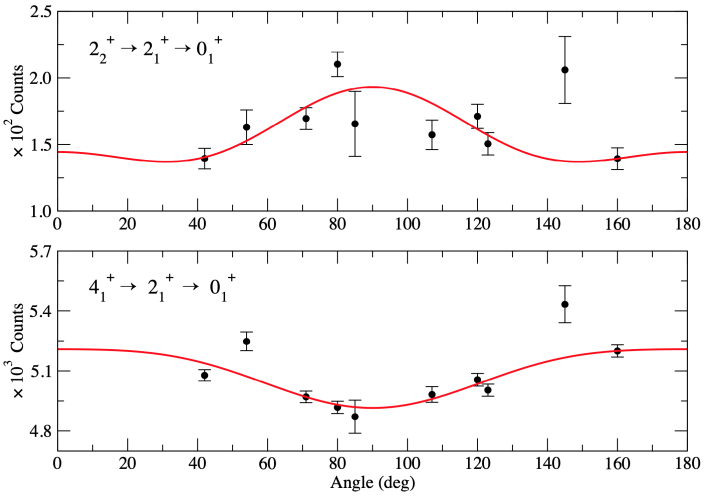

Figure 12: Angular correlations measurement results obtained for ^{154}Er. The bottom panel shows the fit for the $4_1^+ \rightarrow 2_1^+ \rightarrow 0_1^+$ known cascade that highlights the possible errors in the analysis. The top panel shows the fit for the $2_2^+ \rightarrow 2_1^+ \rightarrow 0_1^+$ newly found cascade.

The only state in the γ-band populated enough to perform an angular correlation measurement is the second $I^\pi = 2^+$ state. Even so, the points are very scattered, and we cannot confidently attribute the spin of the level. The points and fit is shown in the top panel of Figure 12. Again, we can see that the point at 144-degree is affected by errors, confirming there is a problem with the detector angle. The best fit possible yields for a_2 and a_4 the following values: a_2 = -0.250 $\pm$ 0.033, a_4 = 0.128 $\pm$ 0.053.

5.5 Results interpretation

The observable for which I calculated the theoretical values is the reduced transition probability B(E2) for each transition in the ground state band up to $I^\pi = 10_1^+$. The obtained values are in overall good agreement with the experimental values for the first

three transitions. Afterward, the reduced transition probability sees a sudden drop, and the theoretical model is not equipped to model this behavior. The interacting boson model predicts a drop in B(E2) values, a feature that gives a better predictive power over the traditional geometric model, but in this case, it seems it starts to drop after the 10^+ state. Even so, the drop for the experimental values is abrupt, and the basic IBA-1 framework cannot model this behavior. The sudden drop can be explained due to the mixing of normal configurations and quasi-particle configurations. In this case, the $I^\pi = 8_2^+$ at 2583.6 keV affects the surrounding levels by lowering the transition rates.

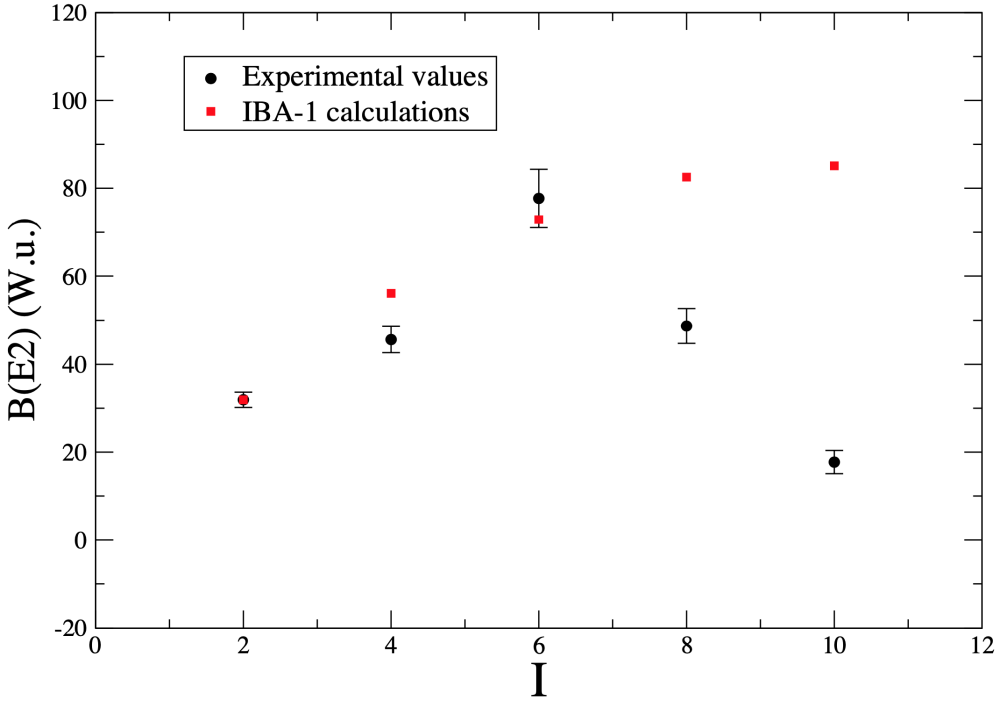

Figure 13: The reduced transition probabilities B(E2) calculated using the IBA-1 framework compared with the experimental values measured in this work.

References

[1] C. Costache, *Advanced spectroscopic techniques applied in the study of nuclear structure*. PhD thesis, Universitatea Politehnica Bucuresti, 2021.

[2] C. Mihai, *Dezvoltari ale metodelor Doppler de determinare a timpilor de viata nucleari*. PhD thesis, Universitatea din Bucuresti, 2011.

[3] S. F. Ashley, *Recoil Distance Doppler Shift Lifetime Measurements of Excited States in 103Pd and 106,107Cd*. PhD thesis, University of Surrey, 2007.

[4] A. Dewald, O. Möller, and P. Petkov, "Developing the recoil distance doppler-shift technique towards a versatile tool for lifetime measurements of excited nuclear states," *Progress in Particle and Nuclear Physics*, vol. 67, no. 3, pp. 786 – 839, 2012.

[5] A. Turturică, C. Costache, P. Petkov, J.-P. Delaroche, M. Girod, J. Libert, G. Cat ă Danil, S. Pascu, C. Mihai, M. Boromiza, D. Bucurescu, C. Clisu, D. Filipescu, N. M. Florea, I. Gheorghe, A. Ionescu, R. Lică, N. M. Mărginean, R. Mărginean, R. E. Mihai, A. Mitu, A. Negret, C. R. Niţă, A. Olăcel, A. Oprea, T. Sava, C. Sotty, L. Stan, I. Ştiru, R. Şuvăilă, S. Toma, G. V. Turturică, and S. Ujeniuc, "Collective properties of neutron-deficient nd isotopes: Lifetime measurements of the yrast states in ^{136}Nd," *Phys. Rev. C*, vol. 103, p. 044306, Apr 2021.

[6] D. Bucurescu, I. Căta-Danil, G. Ciocan, C. Costache, D. Deleanu, R. Dima, D. Filipescu, N. Florea, D. Ghiţă, T. Glodariu, M. Ivaşcu, R. Lică, N. Mărginean, R. Mărginean, C. Mihai, A. Negret, C. Niţă, A. Olăcel, S. Pascu, T. Sava, L. Stroe, A. Şerban, R. Şuvăilă, S. Toma, N. Zamfir, G. Căta-Danil, I. Gheorghe, I. Mitu, G. Suliman, C. Ur, T. Braunroth, A. Dewald, C. Fransen, A. Bruce, Z. Podolyák, P. Regan, and O. Roberts, "The rosphere γ-ray spectroscopy array," *Nuclear Instruments and Methods in Physics Research Section A: Accelerators, Spectrometers, Detectors and Associated Equipment*, vol. 837, pp. 1–10, 2016.

[7] S. RAMAN, C. NESTOR, and P. TIKKANEN, "Transition probability from the ground to the first-excited 2+ state of even–even nuclides," *Atomic Data and Nuclear Data Tables*, vol. 78, no. 1, pp. 1–128, 2001.

[8] J. P. Delaroche, M. Girod, J. Libert, H. Goutte, S. Hilaire, S. Péru, N. Pillet, and G. F. Bertsch, "Structure of even-even nuclei using a mapped collective hamiltonian and the d1s gogny interaction," *Phys. Rev. C*, vol. 81, p. 014303, Jan 2010.

[9] J. Dechargé and D. Gogny, "Hartree-fock-bogolyubov calculations with the $d1$ effective interaction on spherical nuclei," *Phys. Rev. C*, vol. 21, pp. 1568–1593, Apr 1980.

[10] J. Berger, M. Girod, and D. Gogny, "Time-dependent quantum collective dynamics applied to nuclear fission," *Computer Physics Communications*, vol. 63, no. 1, pp. 365–374, 1991.

[11] T. Beck, C. Costache, R. Lică, N. Mărginean, C. Mihai, R. Mihai, O. Papst, S. Pascu, N. Pietralla, C. Sotty, L. Stan, A. Turturică, V. Werner, J. Wiederhold, and W. Witt, "Sorcerer: A novel particle-detection system for transfer-reaction experiments at rosphere," *Nuclear Instruments and Methods in Physics Research Section A: Accelerators, Spectrometers, Detectors and Associated Equipment*, vol. 951, p. 163090, 2020.

[12] P. Möller, R. Bengtsson, B. G. Carlsson, P. Olivius, and T. Ichikawa, "Global calculations of ground-state axial shape asymmetry of nuclei," *Phys. Rev. Lett.*, vol. 97, p. 162502, Oct 2006.

[13] E. Mccutchan, "Nuclear data sheets for a=136," *Nuclear Data Sheets*, vol. 152, pp. 331–667, 2018.

[14] T. Saito, N. Saito, K. Starosta, J. Beller, N. Pietralla, H. Wollersheim, D. Balabanski, A. Banu, R. Bark, T. Beck, F. Becker, P. Bednarczyk, K.-H. Behr, G. Benzoni, P. G. Bizzeti, C. Boiano, A. Bracco, S. Brambilla, A. Brünle, and Q. Zhong, "Yrast and non-yrast 2+ states of 134ce and 136nd populated in relativistic coulomb excitation," *Physics Letters B*, vol. 669, pp. 19–23, 10 2008.

[15] J. Libert, M. Girod, and J.-P. Delaroche, "Microscopic descriptions of superdeformed bands with the gogny force: Configuration mixing calculations in the $a \sim$190 mass region," *Phys. Rev. C*, vol. 60, p. 054301, Sep 1999.

[16] N. M. Florea, L. Stroe, R. Mărginean, D. G. Ghiţă, D. Bucurescu, M. Badea, C. Costache, R. Lică, N. Mărginean, C. Mihai, D. V. Moşu, C. R. Niţă, S. Pascu, and T. Sava, "The status of the target preparation laboratory at ifin-hh bucharest, romania," *Journal of Radioanalytical and Nuclear Chemistry volume*, vol. 305, p. 707–711, 2015.

[17] F. Pühlhofer, "On the interpretation of evaporation residue mass distributions in heavy-ion induced fusion reactions," *Nuclear Physics A*, vol. 280, no. 1, pp. 267–284, 1977.

[18] J. Srebrny, C. Droste, T. Morek, K. Starosta, A. Wasilewski, A. Pasternak, E. Podsvirova, Y. Lobach, G. Hagemann, S. Juutinen, M. Piiparinen, S. Törmänen, and A. Virtanen, "Transition probabilities in negative parity bands of the 119i nucleus," *Nuclear Physics A*, vol. 683, no. 1, pp. 21–47, 2001.

[19] C. Baktash, E. der Mateosian, O. C. Kistner, and A. W. Sunyar, "Irregularities in side-feeding patterns, energies, and multipolarities in the ^{154}Er yrast cascade to spin 36," *Phys. Rev. Lett.*, vol. 42, pp. 637–640, Mar 1979.

[20] C. J. Lister, D. Horn, C. Baktash, E. der Mateosian, O. C. Kistner, and A. W. Sunyar, "High spin states in ^{156}Yb ($n = 86$)," *Phys. Rev. C*, vol. 23, pp. 2078–2085, May 1981.

[21] J. Pedersen, B. B. Back, F. M. Bernthal, S. Bjørnholm, J. Borggreen, O. Christensen, F. Folkmann, B. Herskind, T. L. Khoo, M. Neiman, F. Pühlhofer, and G. Sletten, "Island of high-spin isomers near $n = 82$," *Phys. Rev. Lett.*, vol. 39, pp. 990–993, Oct 1977.

[22] F. S. Stephens, M. A. Deleplanque, R. M. Diamond, A. O. Macchiavelli, and J. E. Draper, "Structural changes in ^{156}Er at high spins," *Phys. Rev. Lett.*, vol. 54, pp. 2584–2587, Jun 1985.

[23] J. Borggreen, G. Sletten, S. Bjørnholm, J. Pedersen, R. Janssens, I. Ahmad, P. Chowdhury, T. Khoo, Y. Chung, and P. Daly, "Nuclear structure effects in the feeding of yrast states of gd, dy and er nuclei," *Nuclear Physics A*, vol. 443, no. 1, pp. 120–134, 1985.

[24] L. A. Bernstein, J. R. Hughes, J. A. Becker, L. P. Farris, E. A. Henry, S. J. Asztalos, B. Cederwall, R. M. Clark, M. A. Deleplanque, R. M. Diamond, P. Fallon, I. Y. Lee, A. O. Macchiavelli, F. S. Stephens, J. A. Cizewski, and W. Younes, "Superdeformation in ^{154}Er," *Phys. Rev. C*, vol. 52, pp. R1171–R1174, Sep 1995.

[25] K. Lagergren, B. Cederwall, T. Bäck, R. Wyss, E. Ideguchi, A. Johnson, A. Ataç, A. Axelsson, F. Azaiez, A. Bracco, J. Cederkäll, Z. Dombrádi, C. Fahlander, A. Gadea, B. Million, C. M. Petrache, C. Rossi-Alvarez, J. A. Sampson, D. Sohler, and M. Weiszflog, "Coexistence of superdeformed shapes in ^{154}er," *Phys. Rev. Lett.*, vol. 87, p. 022502, Jun 2001.

[26] K. S. Toth, D. C. Sousa, J. C. Batchelder, J. M. Nitschke, and P. A. Wilmarth, "Decay properties of ^{154}Tm and observation of fine structure in its α-particle spectrum," *Phys. Rev. C*, vol. 56, pp. 3410–3413, Dec 1997.

[27] P. Aguer, G. Bastin, A. Charmant, Y. El Masri, P. Hubert, R. Janssens, C. Michel, J. Thibaud, and J. Vervier, "Lifetimes of high-spin yrast states in 154er," *Physics Letters B*, vol. 82, no. 1, pp. 55–59, 1979.

[28] D. Ward, J. Sharpey-Schafer, T. Alexander, H. Andrews, O. Häusser, and J. Keinonen, "Remeasurement of lifetimes for high spin states in 154er," *Physics Letters B*, vol. 99, no. 5, pp. 378–382, 1981.

[29] F. A. Beck, J. Dudek, B. Haas, J. C. Merdinger, A. Nourreddine, Y. Schutz, J. P. Vivien, P. Hubert, D. Dassié, G. Bastin, L. Nguyen, J. P. Thibaud, and W. Nazarewicz, "High-spin structure in ^{154}er," *Z. Phys.A Atomic Nuclei*, vol. 319, p. 119–132, 1984.

[30] J. P. Revill, E. S. Paul, X. Wang, M. A. Riley, J. Simpson, R. V. F. Janssens, J. Ollier, A. J. Boston, M. P. Carpenter, C. J. Chiara, C. R. Hoffman, F. G. Kondev, T. Lauritsen, P. J. Nolan, J. M. Rees, S. V. Rigby, C. Unsworth, S. Zhu, and I. Ragnarsson, "Quadrupole moments of coexisting collective shapes at high spin in ^{154}**Er**," *Phys. Rev. C*, vol. 88, p. 031304, Sep 2013.